(Received 24 March 2026, Accepted 8 July 2026, Scheduled 28 July 2026)

Ionic-Ferroelectric Halide Perovskite Artificial Synapses with Dual-Mode Synaptic Plasticity

Dae-Han Kang[1, †], Kwan-Nyeong Kim[1, †], Hea-Lim Park[1, 2, †], Joo Sung Kim[1], Jung-Min Heo[1], Huanyu Zhou[1, 3], Dong-Hyeok Kim[1], Gyeong-Tak Go[1], Ju Yong Park[1], Antonio Facchetti[3], Min Hyuk Park[1], In-Hyeok Park[4], and Tae-Woo Lee[1, 5, 6, *]

[1] *Department of Materials Science and Engineering, Seoul National University 1, Gwanak-ro, Gwanak-gu, Seoul 08826, Republic of Korea*
[2] *Department of Materials Science and Engineering, Seoul National University of Science and Technology 232, Gongneung-ro, Nowon-gu, Seoul 01811, Republic of Korea*
[3] *School of Materials Science and Engineering, Georgia Institute of Technology, Atlanta, GA 30332, USA*
[4] *Graduate School of Analytical Science and Technology and Institute for Sciences of the Universe, Chungnam National University, 99, Daehak-ro, Yuseong-gu, Daejeon 34134, Republic of Korea*
[5] *Research Institute of Advanced Materials, Seoul National University, Seoul 08826, Republic of Korea*
[6] *Interdisciplinary Program in Bioengineering, Institute of Engineering Research, Soft Foundry Seoul National University, Seoul 08826, Republic of Korea*

ABSTRACT: Halide perovskites have demonstrated both short-term and long-term synaptic plasticity behaviors through various physical mechanisms, making them promising materials for neuromorphic electronics. However, most studies rely on distinct materials or device architectures optimized for a single mechanism, limiting the realization of both forms of synaptic plasticity within a unified material system. Here, we report ionic-ferroelectric halide perovskite (IFHP) artificial synapses that integrate two fundamentally different resistance-switching processes within a single material. This functionality is enabled by the ferroelectric Dion-Jacobson perovskite (4-AMP)PbI_4 (4-AMP = 4-(aminomethyl)piperidinium), which exhibits ion-migration-dominated behavior below the coercive voltage ($V_C \sim 3.5$ V) and ferroelectric polarization switching above this threshold. Accordingly, the device exhibits volatile paired-pulse facilitation without stable non-volatile memory retention under sub-coercive stimulation, while exhibiting stable non-volatile memory above V_C. The ferroelectric-polarization-driven long-term plasticity is further supported by extended retention over 2×10^4 s, cycling operation, and device-to-device reproducibility. In addition, the IFHP artificial synapse emulates bio-inspired associative learning and nociceptive sensory functions, highlighting its potential as neuromorphic hardware. These results establish a single-material pathway for voltage-programmable mixed plasticity, addressing a key challenge in halide perovskite neuromorphic hardware.

1. INTRODUCTION

Neuromorphic electronics implement artificial neural networks through distributed, event-driven, and locally adaptive dynamics, offering a pathway toward energy-efficient, scalable, and parallel information processing beyond conventional computing architectures [1–3]. Artificial synaptic devices serve as core elements of neuromorphic hardware by physically modulating ionic or electronic conductance states to emulate short-term and long-term plasticity, thereby enabling in situ memory-processing integration, temporal signal accumulation, adaptive weight updating, and energy-efficient, biologically inspired computation beyond the von Neumann architecture [4–6].

Halide perovskites have recently emerged as compelling active materials for artificial synaptic devices owing to their defect-tolerant band structure, intrinsically coupled ionic-electronic transport, and wide compositional and dimensional tunability [7, 8]. This unique material-level functionality collectively enables low-voltage, analog and history-dependent conductance modulation through controlled ion migration and interfacial polarization dynamics, thereby establishing halide perovskites as a versatile materials platform for energy-efficient synaptic devices and neuromorphic systems [7, 8]. Despite these advantages, the applicability of halide perovskites to neuromorphic systems requires intrinsic coexistence of volatile short-term plasticity (STP) and non-volatile long-term plasticity (LTP), which together provide a physical basis for cooperative learning dynamics across multiple timescales.

To achieve this, diverse switching mechanisms, including metal or halide ion migration [9–12], vacancy-induced interfacial doping [13], and ferroelectric polarization switching [14, 15], have independently enabled either STP or LTP. However, most demonstrations to achieve STP and LTP still depend on separate materials or device architectures specifically engineered for a single mechanism, limiting the implementation of both STP and LTP modes of synaptic plasticity within a unified and compact platform.

* Corresponding author: Tae-Woo Lee (twlees@snu.ac.kr).
† These authors contributed equally.

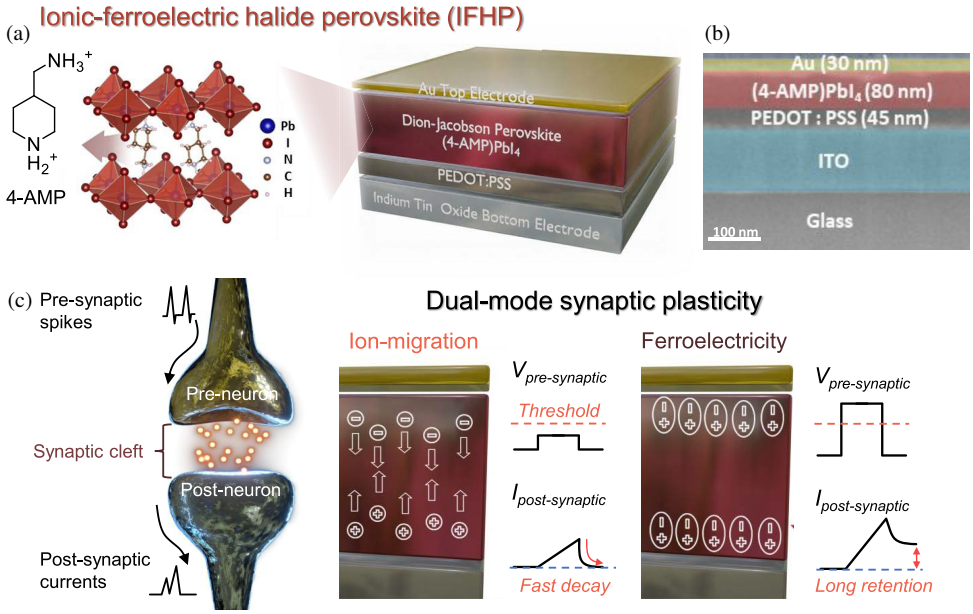

FIGURE 1. Concept of voltage-controlled dual plasticity in the IFHP synaptic device. (a) Schematics of IFHP material and device. (b) A cross-sectional SEM image displays the ITO/PEDOT:PSS/(4-AMP)PbI_4/Au device. (c) Schematic illustration of bias-dependent mechanisms, where ion migration dominates under sub-coercive bias to produce STP, while ferroelectric polarization switching above the coercive voltage induces LTP.

Here, we demonstrate ionic-ferroelectric halide perovskite (IFHP) artificial synapses integrating volatile ion migration and non-volatile ferroelectric switching mechanisms in a single device. This dual-mode synaptic plasticity was enabled by employing the ferroelectric Dion-Jacobson 4-(aminomethyl)piperidine lead iodide [(4-AMP)PbI_4 (4-AMP = 4-(aminomethyl)piperidinium)] halide perovskite, in which volatile halide ion and vacancy migration dominate below the coercive voltage (V_C ~3.5 V) whereas ferroelectric polarization switching is activated above this voltage threshold (Fig. 1). The coexistence of these two voltage-dependent mechanisms enables short-term plasticity without non-volatile retention under sub-coercive voltage conditions and a voltage-dependent increase in residual memory under supra-coercive stimulation.

2. RESULTS AND DISCUSSION

With this ionic-ferroelectric halide perovskite (IFHP), a two-terminal artificial synapse was fabricated using a vertically stacked structure consisting of an indium tin oxide (ITO) bottom electrode, a PEDOT:PSS buffer layer, a 2D ferroelectric halide perovskite active layer, and a gold (Au) top electrode (Figs. 1(a) and 1(b)). In this architecture, the Au top electrode functions as the presynaptic terminal, receiving voltage spikes associated with external stimuli, while the ITO/PEDOT:PSS bottom electrode serves as the postsynaptic node where the excitatory postsynaptic current (EPSC) is monitored.

For characterization, the IFHP films fabricated on glass substrates were prepared by spin-coating a [(4-AMP)PbI_4] solution in *N,N*-dimethylacetamide (DMA) on the desired substrate followed by thermal annealing to promote solvent removal and crystallization. Details of [(4-AMP)PbI_4] synthesis and coating procedures are described in Method section.

We first characterized [(4-AMP)PbI_4] film morphology using scanning electron microscopy (SEM) and atomic force microscopy (AFM). SEM imaging reveals formation of a dense film composed of closely packed grains (Fig. 2(a)). AFM analysis with a line scan profile corroborates the presence of distinct grains and a smooth surface topography with an RMS surface roughness value of 9.34 nm (Fig. 2(b)).

To examine the ferroelectric phase of (4-AMP)PbI_4, we first analyzed the X-ray diffraction (XRD) pattern of the as-synthesized (4-AMP)PbI_4 powder (Fig. 2(c)). The experimental diffraction peaks show agreement with the simulated pattern of monoclinic (4-AMP)PbI_4, indicating that the synthesized compound is consistent with the well-established polar crystal structure associated with ferroelectric behavior [16].

We then investigated the structural characteristics of the spin-coated films using XRD (Fig. 2(d)). The diffraction pattern of the film exhibits a distinct low-angle (100) reflection, which is a characteristic of layered Dion-Jacobson 2D perovskites and indicates preferential out-of-plane stacking of the inorganic layers [16]. The presence of this reflection suggests that the layered perovskite framework is preserved after solution processing and that the films maintain the structural anisotropy required for out-of-plane polarization, while XRD provides structural evidence consistent with the ferroelectric phase.

To further confirm the formation of the perovskite thin film, UV-Vis absorption spectroscopy was performed (Figs. 2(e) and 2(f)). The film exhibits an absorption onset in the visible region at 530 nm. The optical band gap was estimated from the absorption edge using the Tauc relation for a direct transition, yielding a value of 2.34 eV. This value is consistent with previously reported values for ferroelectric (4-AMP)PbI_4 [16], confirming the optical properties of the fabricated film.

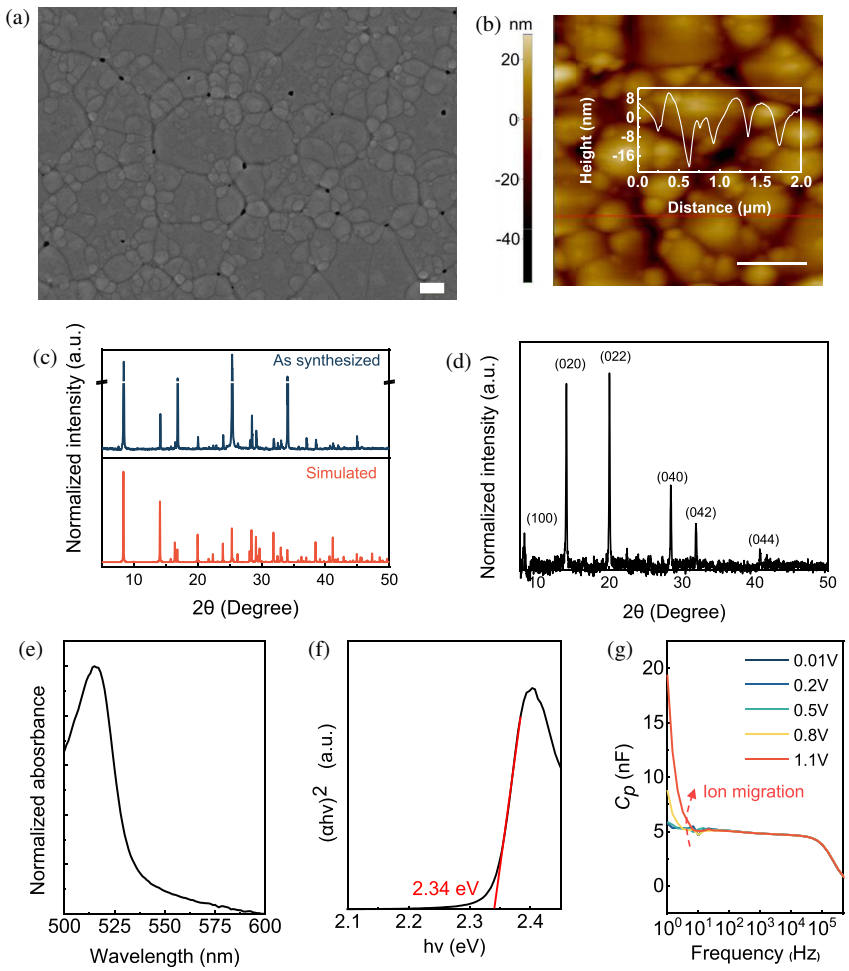

FIGURE 2. Structural, optical, and ionic characterization of (4-AMP)PbI_4 thin films. (a) Scanning electron microscopic image and (b) atomic force microscopy (AFM) topography image of the (4-AMP)PbI_4 thin film. Scale bars: (a) 200 nm and (b) 500 nm. (c) XRD patterns of as-synthesized single crystal powder (top) and the simulated result of the ferroelectric (4-AMP)PbI_4 phase (bottom). (d) XRD pattern of the spin-coated thin film. (e) UV-Vis absorbance spectrum of a (4-AMP)PbI_4 thin film. (f) Tauc plot derived from the absorbance data, yielding an optical band gap of 2.34 eV assuming a direct allowed transition. (g) Capacitance-frequency (C-F) measurements at different voltages.

To investigate the onset of ion migration in the IFHP film, we measured the voltage-dependent capacitance characteristics in the range of 1–10^6 Hz (Fig. 2(g)). In the 1–10 Hz range, where ionic contribution is most pronounced, the capacitance values at 1 Hz for 0.01 V, 0.2 V, and 0.5 V remain nearly identical at approximately 6 nF, indicating that the ionic species are not sufficiently activated under these low-bias conditions. However, once the applied bias reaches 0.8 V, the capacitance increases to ∼9 nF, representing the initial deviation from the baseline and suggesting the onset of field-activated ionic displacement within the dielectric or active layer. At 1.1 V, the capacitance sharply rises to ∼19 nF, suggesting significant ionic redistribution and interfacial polarization within the IFHP film. This voltage-dependent transition identifies ∼0.8 V as the onset voltage at which ion migration begins to contribute to the overall capacitance response. The strong increase at higher bias further supports the bias-driven ionic mobility characteristic of a mixed ionic-electronic system.

To quantify the ferroelectric behavior of (4-AMP)PbI_4 films, we first employed the Positive-Up-Negative-Down (PUND) method to extract the intrinsic polarization response (Figs. 3(a) and 3(b)). The PUND sequence allows separation of ferroelectric switching charges from non-switching capacitive or leakage contributions, thereby enabling the reliable determination of positive and negative remnant polarization values, P_r and P_r^*, respectively [17, 18]. In this method, the effective polarization is calculated by comparing the charge density generated by the switching pulse (P-pulse) with that generated by the subsequent non-switching pulse (U-pulse). The difference between these two quantities directly represents the reversible polarization associated with dipole reorientation. By integrating the current response during each pulse, we obtained the charge per unit area for the P-pulse (Q_P) and U-pulse (Q_U). Subtracting these values yielded a switchable polarization window defined by $P_r - P_r^* = Q_p - Q_u = 1.09\,\mu C\,cm^{-2}$, confirming ferroelectric switching in the film. Notably, a spontaneous polarization of 9.8 $\mu C\,cm^{-2}$ has been reported for the single-crystal form [16], confirming the intrinsically ferroelectric nature of this material system. More broadly, representative 2D Dion-Jacobson and Ruddlesden-Popper halide perovskites reported

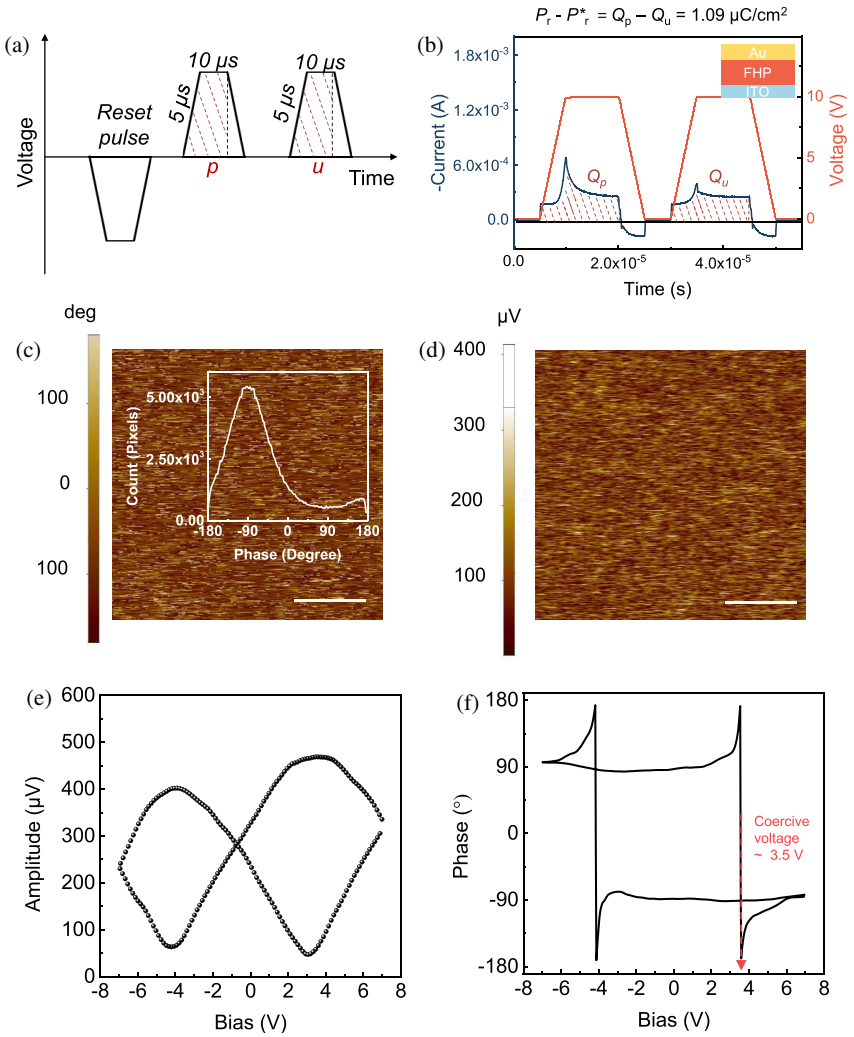

FIGURE 3. Ferroelectric characterization of (4-AMP)PbI_4 thin films. (a) Schematic illustration of the Positive-Up–Negative-Down (PUND) pulse sequence used to separate switching and non-switching polarization components. (b) Extracted polarization response from PUND measurements, yielding $P_r - P_r^*$ of 1.09 μC cm^{-2}. (c) Out-of-plane piezoresponse force microscopy (PFM) phase mapping and phase distribution histogram. Scale bar: 500 nm. (d) Corresponding PFM amplitude mapping. Scale bar: 500 nm. (e) Local PFM switching spectroscopy amplitude loop. (f) Corresponding phase hysteresis loop showing abrupt 180° switching at the V_C.

in the literature exhibit polarization values over a broad range, within which the present system falls. Although the measured polarization is reduced in the thin-film form, it remains sufficient for the intended synaptic operation, thereby supporting the validity of the present synaptic device system (Table S1).

To visualize the presence and spatial coherence of ferroelectric polarization, we conducted out-of-plane piezoresponse force microscopy (PFM). The amplitude and phase mappings reveal the electromechanical response induced by the inverse piezoelectric effect, allowing nanoscale visualization of ferroelectric domains. The phase image and corresponding phase distribution histogram (Fig. 3(c)) display a nearly uniform phase contrast across the scanned area, with a narrow Gaussian-like distribution centered near −90°, suggesting a predominant out-of-plane polar orientation. Such unimodal phase distribution is typical of films possessing vertical ferroelectric polarization; in contrast, centrosymmetric or paraelectric materials typically show a broad, random distribution across the 0–180° range [19, 20]. The amplitude mapping (Fig. 3(d)) also shows a relatively uniform electromechanical response, which is consistent with the presence of a well-aligned polar state.

Local switching spectroscopy PFM measurements were then performed to probe nanoscale polarization reversibility (Figs. 3(e) and 3(f)). The applied tip bias was swept from +7 V to −7 V and then back to +7 V while simultaneously recording amplitude and phase hysteresis loops. The amplitude signal exhibits a characteristic butterfly-shaped curve associated with ferroelectric switching, reflecting the electromechanical response change during polarization reversal near the coercive biases [19, 20]. Correspondingly, the phase loop displays a square-like hysteresis behavior with abrupt 180° switching at coercive voltages (V_C) of approximately −4 V and +3.5 V. These features confirm domain switching driven by an external electric field and unambiguously establish the ferroelectric nature of (4-AMP)PbI_4 layers. The combination of well-defined switching, coercive fields, and reproducible hysteresis

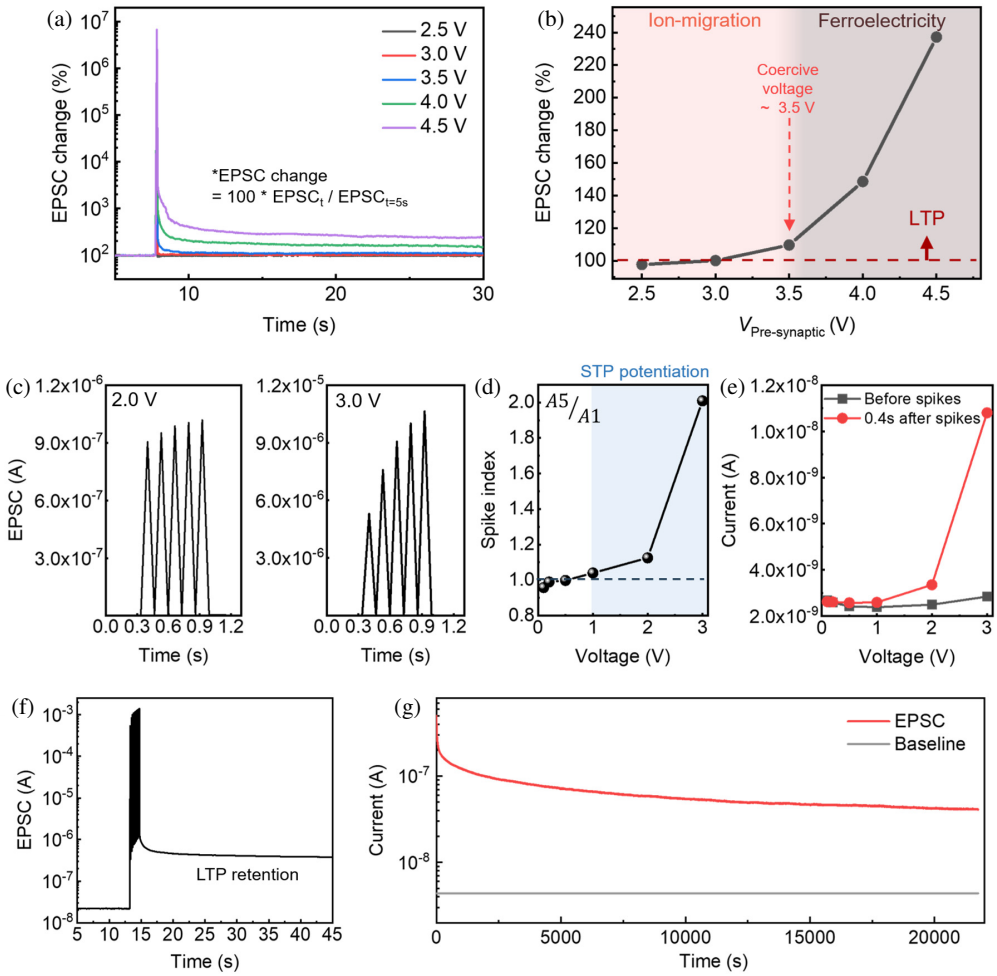

FIGURE 4. Voltage-programmable dual synaptic plasticity in the IFHP device. (a) EPSC responses under different presynaptic voltages. (b) Quantitative EPSC change as a function of presynaptic voltage. (c) EPSC responses to five consecutive presynaptic spikes at 2.0 and 3.0 V, showing voltage-dependent STP potentiation. (d) Spike index as a function of spike voltage, indicating the emergence of STP potentiation in the 1–3 V range. (e) Current levels before and after spike stimulation, showing enhanced post-spike current at higher voltages. (f) LTP response induced by a 5 V spike train, exhibiting non-volatile retention after programming. (g) Long-term retention of the potentiated current state monitored at a read bias of 50 mV.

loops demonstrates that the dipole orientation is stable yet electrically reversible. Consequently, the combined PUND and PFM results confirm intrinsic and switchable ferroelectric polarization in the (4-AMP)PbI_4 thin films, where the V_C marks the transition from ion-migration-dominated sub-coercive modulation to ferroelectric-polarization-dominated switching associated with the non-centrosymmetric monoclinic Pc phase.

The IFHP device exhibits voltage-dependent synaptic plasticity (Fig. 1(c)). At presynaptic spike amplitudes below the $V_C \sim 3.5$ V, the EPSC increases during spike stimulation but rapidly decays back to its baseline after the stimulus is removed, indicating volatile conductance modulation. In contrast, when the presynaptic bias exceeds V_C, the EPSC remains elevated after stimulation, demonstrating non-volatile synaptic weight updates. These distinct behaviors originate from two different mechanisms operating at separate voltage regimes: reversible ion migration dominating below V_C and ferroelectric polarization switching activated above V_C.

The voltage-dependent EPSC modulation quantitatively reveals a clear transition in memory behavior across V_C (Figs. 4(a) and 4(b)). At sub-coercive biases of 2.5 V and 3.0 V, the EPSC change 30 seconds after voltage spike applications shows 97.67% and 100.09%, respectively, indicating negligible LTP and predominantly volatile conductance modulation. At 3.5 V, which corresponds to the coercive voltage identified from PFM measurements, the EPSC change increases to 109.65%, marking the onset of a non-volatile contribution. Above this threshold, a significant enhancement in memory retention is observed, with EPSC change increasing sharply to 148.57% at 4.0 V and 237.16% at 4.5 V. This amplification beyond 3.5 V demonstrates that V_C serves as a physical threshold separating two distinct operating regimes; below the threshold, conductance modulation is governed by reversible ion migration leading to STP, whereas above the threshold, ferroelectric polarization switching is activated, resulting in stable LTP with significantly enhanced memory retention. These results show that the applied voltage determines the dominant mechanism, where the V_C

functions as a threshold separating ion-migration-driven transient modulation from polarization-driven persistent memory, thereby enabling dual plasticity within a single material platform suitable for both sensory processing and computing functions [5, 21].

The repeated 3 V–5 V spike-train measurements further clarify the coupling between the two plasticity mechanisms (Fig. S1). Before ferroelectric programming, the 3 V spike train produces a transient potentiation response, consistent with sub-coercive ion migration and volatile interfacial field modulation (Fig. S1(a)). In contrast, after the 5 V spike train updates the device into a ferroelectric LTP state, the subsequent 3 V stimulation induces only negligible additional potentiation, while the retention current generated by the 5 V update is preserved (Fig. S1(a)). This behavior suggests that, under the present pulse condition, the ferroelectric-polarization-induced internal field appears to dominate the post-programmed conductance state, making the effective contribution of ionic modulation less pronounced than that of the ferroelectric-polarization-induced field (Fig. S1(b)). Because the 3 V pulses remain below the coercive voltage, they are unlikely to substantially alter the remnant polarization, which may explain why the LTP retention is not significantly affected by subsequent STP-level stimulation (Fig. S1(b)). These results suggest a coupled ferroelectric-ionic operation rather than completely independent mechanisms: ion migration primarily contributes to volatile STP before ferroelectric programming, whereas ferroelectric polarization mainly governs the non-volatile LTP state after supra-coercive stimulation and reduces the observable ionic STP modulation.

Voltage-dependent STP characteristics of the IFHP artificial synapse were investigated by applying five consecutive presynaptic spikes with different amplitudes (Figs. 4(c)–(e) and Fig. S2). At low spike voltages below 1 V, the device showed only weak EPSC modulation with spike indices close to unity, indicating negligible spike-dependent potentiation and no clear evidence of synaptic plasticity. In contrast, clear potentiation emerged when the spike voltage reached 1 V, where the spike index increased to 1.04, and further increased gradually to 1.12 and 2.01 at 2 and 3 V, respectively (Fig. 4(d)). Furthermore, the retained current also increases with the input voltages (Fig. 4(e)). This voltage-dependent enhancement indicates that sufficient sub-coercive bias activates reversible ion migration and transient interfacial accumulation, enabling short-term synaptic potentiation. Therefore, the 1 to 3 V regime is suitable for ion-migration-driven STP operation in artificial synapses, whereas lower voltages are more appropriate for non-synaptic readout operation.

To evaluate the cycling behavior of ion-migration-driven STP, repetitive 2 V spike trains consisting of five spikes were applied to the IFHP device (Fig. S3). During the first 10 cycles, the EPSC responses were well preserved, showing reproducible spike-dependent potentiation and relaxation. This result indicates that sub-coercive stimulation can reliably induce volatile STP through reversible ion redistribution in the perovskite film under repeated operation. After extended cycling beyond 100 cycles, the overall EPSC level gradually increased. This trend suggests that repeated stimulation may induce a slight cumulative change in the ionic or interfacial state of the halide perovskite film, such as partial ion accumulation, defect-assisted interfacial doping, or a gradual decrease in the injection barrier. Nevertheless, the stable STP behavior during the initial cycling regime confirms the feasibility of reversible ion-migration-based short-term plasticity.

To evaluate ferroelectric-polarization-driven LTP and its device-to-device reproducibility, 5 V spike trains consisting of 20 pulses were applied to multiple IFHP devices, and the resulting EPSC responses were monitored at a read bias of 50 mV (Fig. 4(f) and Fig. S4). All measured devices exhibited a pronounced current increase during programming, followed by a retained current after removal of the spike train, confirming the formation of non-volatile potentiated states. The extracted EPSC change at $t = 40$ s was $1335 \pm 360\%$ across 10 different devices, indicating reproducible ferroelectric-polarization-driven LTP in solution-processed IFHP thin-film devices. Although device-to-device variation remains, it is reasonable for proof-of-concept perovskite thin-film electronics and can be further reduced by optimizing film thickness, crystallinity, grain structure, defect density, substrate surface treatment, electrode/transport-layer interfaces, device geometry, and encapsulation. These results support the feasibility of reproducible non-volatile synaptic weight modulation in the IFHP artificial synapse, while further process optimization is expected to improve device uniformity for practical neuromorphic hardware applications.

To evaluate the cyclic LTP behavior of the IFHP device, repeated voltage spike trains were applied (Fig. S5). Each stimulation cycle consisted of 100 consecutive voltage pulses with an amplitude of 5 V and an inter-pulse interval of approximately 0.18 s, corresponding to a total stimulation duration of approximately 17 s per cycle. After each spike train, the device was allowed to relax for approximately 12 s, and the post-stimulation conductance was monitored at a read bias of 50 mV. The device exhibited a clear cycle-dependent potentiation behavior. During the initial cycles, the EPSC increased progressively with repeated stimulation, indicating gradual conductance modulation and analog-like synaptic weight updates. As the number of cycles increased, the conductance modulation became less pronounced and gradually approached a saturated state after approximately 200 to 300 cycles. This saturation behavior suggests that the available ferroelectric polarization or interfacial modulation states were progressively occupied under the present programming condition.

To further assess the retention characteristics of ferroelectric-polarization-driven LTP, the IFHP device was programmed using a 5 V spike train consisting of 100 consecutive pulses, and the memory current was subsequently monitored at a read bias of 50 mV (Fig. 4(g)). After programming, the device exhibited a clear increase in current compared with the initial baseline, indicating successful formation of a non-volatile potentiated state. The memory current remained higher than the baseline throughout the measurement. Notably, the elevated current state was maintained over 2×10^4 s, demonstrating stable long-term retention after supra-coercive stimulation. This per-

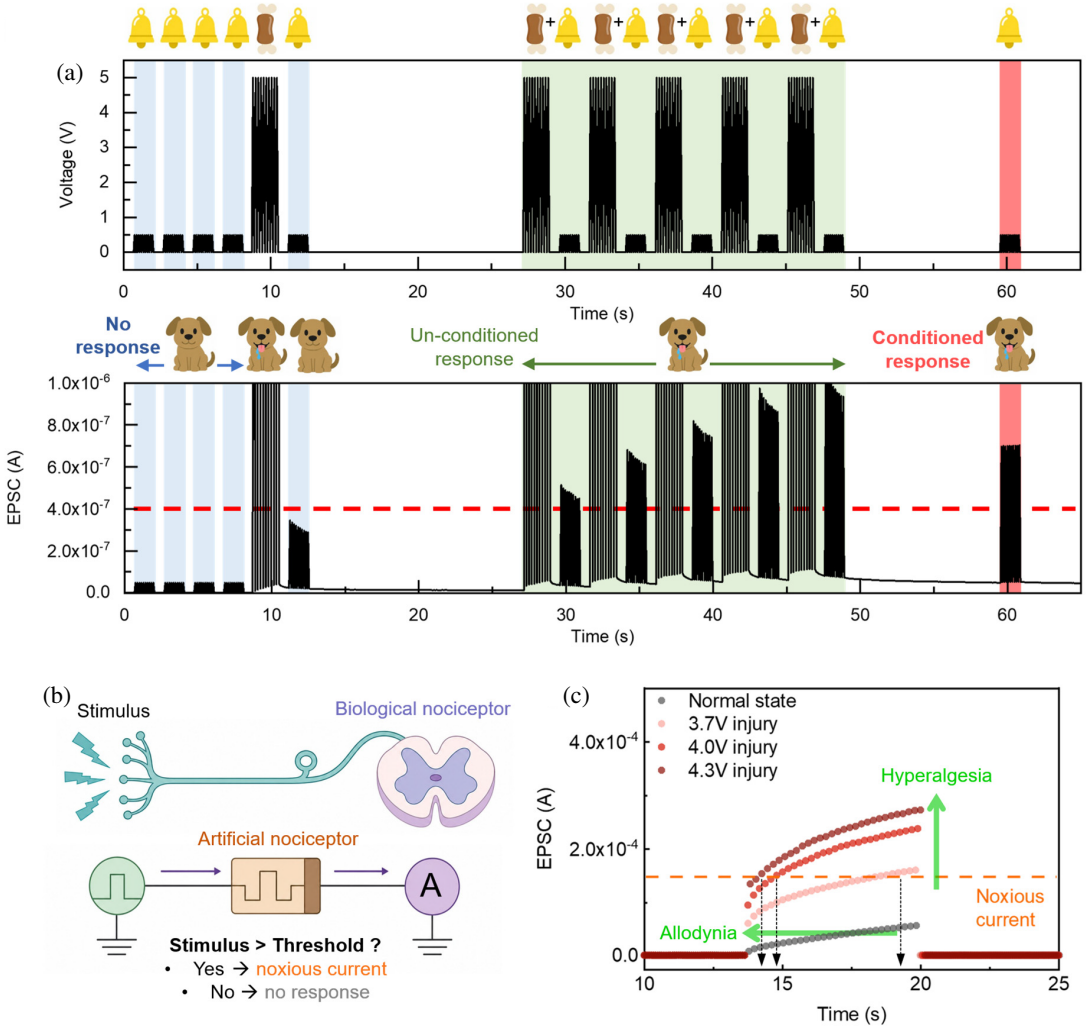

FIGURE 5. Bio-inspired learning and pain response of the IFHP devices. (a) Pavlovian associative learning, where paired bell and food stimuli enable the initially ineffective bell stimulus to generate a conditioned response above the threshold. (b) Schematic of biological and artificial nociceptors with threshold-dependent noxious current generation. (c) Injury-induced sensitization showing allodynia- and hyperalgesia-like EPSC enhancement after injury pulses.

sistent conductance state confirms that the 5 V spike train effectively induces ferroelectric-polarization-driven LTP switching, enabling robust non-volatile memory behavior in the IFHP artificial synapse.

To demonstrate associative learning in the IFHP artificial synapse, a Pavlov's dog conditioning experiment was emulated using two presynaptic inputs with different spike amplitudes (Fig. 5(a)) [22]. A weak 0.5 V spike, representing the bell stimulus, initially produced negligible EPSC at a read voltage of 50 mV and did not exceed the response threshold of 400 nA, corresponding to no response. In contrast, a strong 5 V spike, representing the food stimulus, generated a pronounced EPSC above the threshold, corresponding to an unconditioned response. After repeated paired training with the 0.5 V bell stimulus and the 5 V food stimulus, the synaptic weight was progressively strengthened, and the previously ineffective 0.5 V bell stimulus alone became capable of generating an EPSC above the threshold. This transition from no response to a conditioned response indicates that the artificial synapse can associate a weak neutral stimulus with a strong unconditioned stimulus through spike-dependent conductance modulation. The result demonstrates associative learning behavior in the IFHP device, enabled by the coexistence of volatile ionic modulation and non-volatile ferroelectric memory under low read-bias operation.

Biological nociceptors are specialized sensory receptors that detect potentially harmful stimuli, such as excessive pressure, heat, or chemical irritation, and transmit pain signals to the nervous system only when the stimulus exceeds a critical threshold [23, 24]. Unlike ordinary sensory receptors, nociceptors provide protective signal-processing functions, including threshold activation, sensitization after injury, and enhanced response to repeated harmful stimuli. Memristor-based artificial nociceptors can emulate these functions through threshold switching and history-dependent conductance modulation, providing an efficient hardware platform for protective sensory systems in neuromorphic electronics, electronic skin, and intelligent robotics (Fig. 5(b)) [23, 24].

To evaluate nociceptive behavior in the artificial synapse, the EPSC response was measured by applying 3.0 V and 4.17 Hz spikes before and after the application of injury pulses with different amplitudes (Fig. 5(c)). In the normal state (pristine device), the device showed only a weak EPSC response below the defined noxious current threshold (150 μA), indicating that mild stimulation did not generate a pain-like output. After applying injury pulses of 3.7, 4.0, and 4.3 V, the EPSC response to the same sensory stimulation was markedly enhanced and exceeded the noxious current threshold. In particular, stronger injury pulses produced higher EPSC responses and shorter onset times, demonstrating hyperalgesia- and allodynia-like behavior. The reduced response threshold after injury indicates allodynia, whereas the increased EPSC amplitude under the same stimulation condition indicates hyperalgesia. These results demonstrate that the device emulates key biological nociceptor functions, including threshold-dependent pain perception, injury-induced sensitization, hyperalgesia, and allodynia.

3. CONCLUSION

In summary, we demonstrate a 2D perovskite material platform that supports both STP and LTP within a single device. The [(4-AMP)PbI_4] Dion-Jacobson perovskite films were fabricated through controlled synthesis and solution processing, forming uniform thin films with a preserved ferroelectric phase. Electrical characterization indicates ion migration from low-frequency C-F measurements while PUND analysis confirms intrinsic and switchable ferroelectric polarization with a switchable polarization $P_r - P_r^*$ of 1.09 μC cm^{-2}. PFM measurements further reveal uniform out-of-plane domains and clear 180° phase switching near the coercive voltage ($V_C \sim 3.5$ V). These coupled ionic and ferroelectric properties allow voltage-programmable synaptic plasticity: sub-coercive stimulation induces volatile STP, whereas supra-coercive stimulation produces stable non-volatile LTP. The ferroelectric-polarization-driven LTP state is further supported by extended retention over 2×10^4 s, cycling measurements, and device-to-device reproducibility. In addition, the IFHP artificial synapse emulates bio-inspired associative learning and nociceptive sensory functions, including conditioned response generation and injury-induced sensitization. This work provides a single-material route toward voltage-programmable mixed plasticity for perovskite-based neuromorphic hardware.

ACKNOWLEDGEMENT

D.-H. Kang, K.-N. Kim and H.-L. Park contributed equally to this work. This research was supported by the Pioneer Research Center Program through the National Research Foundation of Korea funded by the Ministry of Science and ICT (MSIT) (RS-2022-NR067540). This work was also supported by the National Research Foundation of Korea (NRF) grant funded by the Ministry of Science and ICT (MSIT) (RS202500560490). This research was supported by Seoul National University of Science and Technology.

REFERENCES

[1] Kumar, S., X. Wang, J. P. Strachan, Y. Yang, and W. D. Lu, "Dynamical memristors for higher-complexity neuromorphic computing," *Nature Reviews Materials*, Vol. 7, No. 7, 575–591, Apr. 2022.

[2] Schuman, C. D., S. R. Kulkarni, M. Parsa, J. P. Mitchell, P. Date, and B. Kay, "Opportunities for neuromorphic computing algorithms and applications," *Nature Computational Science*, Vol. 2, No. 1, 10–19, Jan. 2022.

[3] Kudithipudi, D., C. Schuman, C. M. Vineyard, T. Pandit, C. Merkel, R. Kubendran, J. B. Aimone, G. Orchard, C. Mayr, R. Benosman, *et al.*, "Neuromorphic computing at scale," *Nature*, Vol. 637, No. 8047, 801–812, Jan. 2025.

[4] Marković, D., A. Mizrahi, D. Querlioz, and J. Grollier, "Physics for neuromorphic computing," *Nature Reviews Physics*, Vol. 2, No. 9, 499–510, Jul. 2020.

[5] Choi, Y., D. H. Ho, S. Kim, Y. J. Choi, D. G. Roe, I. C. Kwak, J. Min, H. Han, W. Gao, and J. H. Cho, "Physically defined long-term and short-term synapses for the development of reconfigurable analog-type operators capable of performing health care tasks," *Science Advances*, Vol. 9, No. 27, eadg5946, Jul. 2023.

[6] Sung, M.-J., K.-N. Kim, C. Kim, H.-H. Lee, S.-W. Lee, S. Kim, D.-G. Seo, H. Zhou, and T.-W. Lee, "Organic artificial nerves: Neuromorphic robotics and bioelectronics," *Chemical Reviews*, Vol. 125, No. 5, 2625–2664, 2025.

[7] Vasilopoulou, M., A. R. b. M. Yusoff, Y. Chai, M.-A. Kourtis, T. Matsushima, N. Gasparini, R. Du, F. Gao, M. K. Nazeeruddin, T. D. Anthopoulos, and Y.-Y. Noh, "Neuromorphic computing based on halide perovskites," *Nature Electronics*, Vol. 6, No. 12, 949–962, Dec. 2023.

[8] Das, D., D. S. Assi, S. Kazim, V. A. L. Roy, and S. Ahmad, "Decoding halide perovskites for neuromorphic and memristive devices," *Materials Horizons*, Vol. 12, No. 20, 8430–8459, 2025.

[9] Kim, S. J., I. H. Im, J. H. Baek, S. Choi, S. H. Park, D. E. Lee, J. Y. Kim, S. Y. Kim, N.-G. Park, D. Lee, J. J. Yang, and H. W. Jang, "Linearly programmable two-dimensional halide perovskite memristor arrays for neuromorphic computing," *Nature Nanotechnology*, Vol. 20, No. 1, 83–92, Jan. 2025.

[10] Kim, S.-I., Y. Lee, M.-H. Park, G.-T. Go, Y.-H. Kim, W. Xu, H.-D. Lee, H. Kim, D.-G. Seo, W. Lee, and T.-W. Lee, "Dimensionality dependent plasticity in halide perovskite artificial synapses for neuromorphic computing," *Advanced Electronic Materials*, Vol. 5, No. 9, 1900008, Sep. 2019.

[11] John, R. A., Y. Demirağ, Y. Shynkarenko, Y. Berezovska, N. Ohannessian, M. Payvand, P. Zeng, M. I. Bodnarchuk, F. Krumeich, G. Kara, I. Shorubalko, M. V. Nair, G. A. Cooke, T. Lippert, G. Indiveri, and M. V. Kovalenko, "Reconfigurable halide perovskite nanocrystal memristors for neuromorphic computing," *Nature Communications*, Vol. 13, No. 1, 2074, Apr. 2022.

[12] Lee, S. H., M. J. Lee, H. Ahn, J.-S. Park, S. J. Kim, K. Lee, T. H. Kim, G. M. Lee, K. Kim, and J. W. Shim, "Synaptic plasticity modulation in Dion-Jacobson perovskite artificial synapses enabled by crystallographic orientation control," *Small*, Vol. 21, No. 34, 2504328, Aug. 2025.

[13] Xu, W., H. Cho, Y.-H. Kim, Y.-T. Kim, C. Wolf, C.-G. Park, and T.-W. Lee, "Organometal halide perovskite artificial synapses," *Advanced Materials*, Vol. 28, No. 28, 5916–5922, 2016.

[14] Xu, H., F. Sun, E. Li, W. Guo, L. Hua, R. Wang, W. Li, J. Chu, W. Liu, J. Luo, and Z. Sun, "Ferroelectric perovskite/MoS_2 channel heterojunctions for wide-window nonvolatile memory and neuromorphic computing," *Advanced Materials*, Vol. 37,

No. 4, 2414339, Jan. 2025.

[15] Muddam, R. S. and L. K. Jagadamma, "Ferroelectric polarization in 2D halide hybrid perovskites: Influence on bulk crystals, thin films, and applications," *Journal of Materials Chemistry C*, Vol. 13, No. 21, 10 488–10 506, 2025.

[16] Park, I.-H., Q. Zhang, K. C. Kwon, Z. Zhu, W. Yu, K. Leng, D. Giovanni, H. S. Choi, I. Abdelwahab, Q.-H. Xu, T. C. Sum, and K. P. Loh, "Ferroelectricity and Rashba effect in a two-dimensional Dion-Jacobson hybrid organic-inorganic perovskite," *Journal of the American Chemical Society*, Vol. 141, No. 40, 15 972–15 976, 2019.

[17] Parsonnet, E., Y.-L. Huang, T. Gosavi, A. Qualls, D. Nikonov, C.-C. Lin, I. Young, J. Bokor, L. W. Martin, and R. Ramesh, "Toward intrinsic ferroelectric switching in multiferroic $BiFeO_3$," *Physical Review Letters*, Vol. 125, No. 6, 067601, 2020.

[18] Grigoriev, A., M. M. Azad, and J. McCampbell, "Ultrafast electrical measurements of polarization dynamics in ferroelectric thin-film capacitors," *Review of Scientific Instruments*, Vol. 82, No. 12, 124704, Dec. 2011.

[19] Seol, D., G. S. Han, C. Bae, H. Shin, H. S. Jung, and Y. Kim, "Screening effect on photovoltaic performance in ferroelectric $CH_3NH_3PbI_3$ perovskite thin films," *Journal of Materials Chemistry A*, Vol. 3, No. 40, 20 352–20 358, 2015.

[20] Kim, Y.-J., T.-V. Dang, H.-J. Choi, B.-J. Park, J.-H. Eom, H. Song, D. Seol, Y. Kim, S.-H. Shin, J. Nah, and S.-G. Yoon, "Piezoelectric properties of $CH_3NH_3PbI_3$ perovskite thin films and their applications in piezoelectric generators," *Journal of Materials Chemistry A*, Vol. 4, No. 3, 756–763, 2016.

[21] Lee, S.-W., K.-N. Kim, S. Ma, S. Ahn, D. Choi, M.-J. Sung, C.-Y. Song, J.-Y. Sun, and T.-W. Lee, "Physically reconfigurable synaptic plasticity and learning in stretchable neuromorphic systems," *Materials Horizons*, Vol. 13, No. 8, 3868–3879, 2026.

[22] He, N., F. Ye, J. Liu, T. Sun, X. Wang, W. Hou, W. Shao, X. Wan, Y. Tong, F. Xu, and Y. Sheng, "Multifunctional Ag-In-Zn-S/$Cs_3Cu_2Cl_5$-based memristors with coexistence of non-volatile memory and volatile threshold switching behaviors for neuroinspired computing," *Advanced Electronic Materials*, Vol. 9, No. 3, 2201038, Mar. 2023.

[23] John, R. A., N. Yantara, S. E. Ng, M. I. B. Patdillah, M. R. Kulkarni, N. F. Jamaludin, J. Basu, *et al.*, "Diffusive and drift halide perovskite memristive barristors as nociceptive and synaptic emulators for neuromorphic computing," *Advanced Materials*, Vol. 33, No. 15, 2007851, Apr. 2021.

[24] Wang, Y., Q. Ran, T. Chen, W. Zhang, and K. Zhang, "Lead-free halide perovskite-based flexible memristor for an artificial mechano-nociceptive system," *The Journal of Physical Chemistry Letters*, Vol. 16, No. 12, 3177–3184, Mar. 2025.